



The Stuart–Landau model applied to wake transition revisited

Mark C. Thompson^a, Patrice Le Gal^{b,*}

^a Department of Mechanical Engineering, Monash University, Melbourne, 3800, Australia

^b Institut de recherche sur les phénomènes hors équilibre, 49, rue F. Joliot-Curie, BP 146, 13384 Marseille cedex 13, France

Received 11 April 2003; received in revised form 18 September 2003; accepted 18 September 2003

Abstract

Following previous experimental and computational studies, this article further investigates the applicability of the Stuart–Landau equation to describe the Hopf bifurcation occurring for flow past a circular cylinder. It is shown that when the amplitude variable is taken as the transverse velocity component at a point in the wake, the so-called Landau constant varies considerably with position and importantly is generally far from constant during the saturation phase of wake development. The variation with downstream distance is quantified. However, it is found that the Landau constant *at saturation* is indeed a position-independent constant and this value is close to that generally measured previously both experimentally and numerically. It is shown that if the amplitude variable is taken as the lift coefficient of the cylinder (a global variable) then the same Landau constant is measured at saturation and the zero amplitude Landau constant corresponds to that for the transverse velocity at the back of the cylinder. These findings are used to interpret the wake behaviour of a transversely oscillating circular at subcritical Reynolds numbers. © 2003 Elsevier SAS. All rights reserved.

1. Introduction

The complex Stuart–Landau equation has been widely used to model supercritical bifurcations occurring in flow systems when a control parameter exceeds a critical value. Typical examples include: the transition from steady flow to vortex shedding (i.e., the Hopf bifurcation) in the wake of a circular cylinder [1–6], the regular bifurcation (i.e., steady to steady) of a sphere wake leading to the beautiful two-tailed structure as shown by Margarvey and Bishop [7,8] (see also, e.g., [9,10]); the Hopf bifurcation of the sphere wake [9,11,12]; and the transition to three-dimensional *mode B* shedding of a two-dimensional circular cylinder wake [13]. However, not all flow transitions are governed by the cubic form of the Stuart–Landau model, for instance, the initial three-dimensional transition of a circular cylinder wake from the two-dimensional Bénard–von Karman wake is *subcritical* and hence requires the retention of at least quintic terms to model the approach to the saturated state [14]. In practice, this is indicated by the observation that the transition is hysteretic, or through a discontinuous change in flow parameters such as Strouhal number or the drag coefficient [15,16]. These successes have been achieved despite an incomplete mathematical foundation for the Stuart–Landau model.

A key reason for studying the (Stuart–)Landau model is that, because it is amenable to straight-forward mathematical analysis, it can predict the behaviour of, and provides important insight into, complex flow systems. For instance, Landau models can be coupled together to describe the wake dynamics of interacting cylinder or sphere wakes [17,18]. The model also provides a starting point for the Ginzburg–Landau model describing aspects of the two-dimensional shedding from a circular cylinder, such as phase transitions, oblique shedding and chevron patterns [19–21]. The model can be extended to describe interacting wake modes such as the two initial three-dimensional circular cylinder wake modes [22]. In theory, it can also be extended to wake flows from forced or freely-oscillating bodies. For example, it was applied to predict the asymptotic wake

* Corresponding author.

E-mail address: Patrice.le-gal@irphe.univ-mrs.fr (P. Le Gal).

states of a circular cylinder wake under transverse forcing by Le Gal et al. [23]. Note that for forced Hopf oscillators, a complete mathematical analysis of the different solutions has been provided by Gambaudo [24].

The aim of the present paper is to re-examine the application of the Stuart–Landau model to the Hopf bifurcation of the circular cylinder wake. The work of Dusek et al. [1] showed that the model accurately describes the observed response when the Reynolds number is restricted to be within 10% of the critical value. These authors used the transverse velocity on the wake centreline as the Landau model variable. For points on the wake centreline, the transverse velocity is zero prior to transition, and hence this provides a direct measure of the growth of the instability. Importantly they found that the *Landau constant* indeed appeared to be a constant at all sampled points in the wake. (Interestingly, it will be shown later in this paper that the situation is somewhat more complicated). Zielinska and Wesfried [6] showed universal global mode behaviour with Reynolds number of the transverse velocity component on the centreline, provided the velocity is normalised by its (Reynolds-number dependent) maximum value and position is rescaled by the length to the position of the velocity maximum. The applicability of the model could then be extended to approximately to 30% in excess of the critical value. While this is advantageous in terms of validity of the model, it is restrictive in that the maximum velocity and its position are not known a priori. Another possible choice for the Landau variable is to associate it with a global measure of the perturbation amplitude. This is also problematic because generally this requires an integration over a near-infinite domain; difficult to achieve both experimentally or numerically! In this paper, we initially focus on the local measure of the transverse velocity component at different points in the wake and then examine the predictions for a global variable: the lift coefficient.

In the following sections we briefly review the theory, describe the numerical approach adopted and analyse the numerical data in terms of the Landau model.

2. Theory

2.1. The Stuart–Landau equation

The complex Stuart–Landau equation is given by

$$\frac{dA}{dt} = (\gamma + i\omega)A - (c_R + ic_I)|A|^2A + \dots, \quad (1)$$

in which A is a complex-valued function of time t and the parameters γ , ω , c_R and c_I are all real. The Landau constant, usually denoted by c , is given by $c = c_I/c_R$ in this formulation. The equation is generally truncated after the cubic term as is the usual case for supercritical transitions since the cubic term is nominally sufficient for limiting the initial exponential growth and causing saturation. This is the case for the Hopf bifurcation, i.e., the transition to periodic shedding in the circular cylinder wake. Importantly, the real part of the cubic coefficient is positive so that this term is responsible for saturation. Also note that only odd terms in the (complex) amplitude can appear on the right-hand side [25].

Eq. (1) represents the normal form of the Hopf bifurcation which occurs at the critical value of the parameter $\gamma = 0$. For $\gamma < 0$, the null solution $A = 0$ is a stable solution. For a circular cylinder, the flow corresponds to steady flow with attached eddies at the rear of the cylinder. For $\gamma > 0$, this base state loses its stability and the solution settles down to a time-periodic state (corresponding to Bérnard–von Karman vortex shedding). If only the linear and cubic terms are considered, the saturation amplitude is given by $|A| = (\gamma/c_R)^{1/2}$, and the angular frequency at saturation is given by $\omega - \gamma c$. The time-scale for the transient to leave the null solution is given by γ^{-1} (e.g., [1]).

In general, the parameters in this equation may be a function of Reynolds number although it is hoped that the dependence is weak, except for γ which changes from negative to positive at transition. Also, if A is taken as a local quantity, such as the transverse velocity component, the coefficients may be function of position. It is found that γ and ω are independent of position close to transition, this can be justified both from measurements and on theoretical grounds according to the fact that an absolute instability appears and lets a global mode to take place in the flow. For the analysis presented here we take the coefficients c_R and c_I to depend on $|A|^2$. This is equivalent to including higher-order terms in the equation but allows us instead to focus on the constancy of these parameters during the exponential growth and saturation phases of the transition. To reiterate, for the analysis presented in this article we explicitly truncate Eq. (1) to include only linear and cubic terms. The effect of higher-order terms is then implicitly included by allowing the real and imaginary cubic coefficients to depend on $|A|^2$. Note that in terms of this truncated model, the real and imaginary cubic coefficients at zero amplitude correspond to the cubic coefficients of the original (untruncated) expansion.

To proceed with the analysis of the Landau model, it helps to write $A(t)$ in the form

$$A(t) = \rho(t) e^{i\phi(t)}, \quad (2)$$

where $\rho(t) = |A(t)|$ is the real and non-negative amplitude of the complex function A , and $\phi(t)$ is its phase (also real). Substitution into Eq. (1) results in the pair of equations

$$\frac{d \log \rho}{dt} = \gamma - c_R(\rho^2, \zeta) \rho^2 \quad (3)$$

and

$$\dot{\phi} = \omega - c_I(\rho^2, \zeta) \rho^2. \quad (4)$$

Again note that the cubic coefficients are now written as explicit functions of the time-dependent amplitude ($\rho = |A|$). They are also a function of position ($\zeta = x/R$) if we use the transverse velocity component as the Landau complex amplitude variable.

If $\rho_{\text{sat}}(\zeta)$ is the amplitude at saturation at any point, then from Eq. (3), this can be written in terms of the model parameters as $\rho_{\text{sat}}^2 = \gamma / c_R(\rho_{\text{sat}}^2, \zeta)$. In addition, if we make the physically reasonable assumption that the flow is *locked* at all points once that flow has reached the saturated state (see later for verification), and if ϕ_{sat} is the position-independent saturated angular frequency, then $\dot{\phi}_{\text{sat}} = \omega - c_I(\rho_{\text{sat}}^2, \zeta) \rho_{\text{sat}}^2(\zeta)$. Using the previous result,

$$\Delta\omega = \dot{\phi} - \omega = \frac{c_I(\rho_{\text{sat}}^2, \zeta)}{c_R(\rho_{\text{sat}}^2, \zeta)} \gamma = c_{\text{sat}} \gamma. \quad (5)$$

Here, $\Delta\omega$ represents the shift in angular frequency from that during the linear phase. Since ω , γ and $\dot{\phi}_{\text{sat}}$ are all position independent (due to the initial flow locking and locking at saturation), $c_{\text{sat}}(\rho_{\text{sat}}^2, \zeta) \equiv (c_I(\rho_{\text{sat}}^2, \zeta)) / c_R(\rho_{\text{sat}}^2, \zeta)$ must be position-independent. Using numerical experiments, Dusek et al. [1] found that the Landau constant was approximately constant, however, the present analysis indicates that very simple and reasonable assumptions, i.e., initial and final flow locking and no quadratic dependence in Landau model, effectively require the Landau constant at saturation to be independent of position. This will be examined numerically in the results section. Note that this analysis says nothing about the behaviour of the Landau constant during the initial growth phase of the instability.

3. Results

In this section we examine the Hopf bifurcation in some detail attempting to quantify the model coefficients as the wake undergoes transition, the instability grows linearly and finally reaches saturation.

3.1. Numerical methodology

We describe a series of simulations which extend the work of Dusek et al. [1]. The spectral-element method is used to simulate the flow at post-critical Reynolds numbers. The specific implementation is described in Thompson et al. [26]. This implementation achieves second-order time accuracy and spectral spatial convergence as the number of nodes per element is increased, as is common for global spectral methods [27]. The software has been successfully used on a number of related problems, e.g., flow past plates, and three-dimensional circular cylinder wake transition [26]. Care has been taken to verify that both the grid resolution and domain size are sufficient to obtain accurate results, even though, as pointed out by Dusek et al. [1], the similar results are achieved for less refined meshes and smaller domains. The domain size has the following characteristic dimensions: inflow length = distance to side boundaries = $50D$, and outflow length = $85D$. Resolution and domain size studies indicate the accuracy of the predictions is better than 1%.

The behaviour of the flow is monitored by recording the velocity components at fixed points downstream along the wake centreline, and by recording the lift and drag force on the cylinder. Both the transverse component of the velocity along the wake centreline and the lift coefficient (per unit length) are zero in the pre-transition state. In the following sections the results for the transverse velocity are discussed first.

The saturated wake state at $Re = 48$ is shown in terms of the vorticity field in Fig. 1. This is only about 3% above the critical Reynolds number of $Re = 46.4$ found for the present simulations. The exact transition Reynolds number is slightly dependent on domain blockage; Dusek et al. [1] found a critical value of $Re = 46.1$.



Fig. 1. Vorticity field in the wake at $Re = 48$.

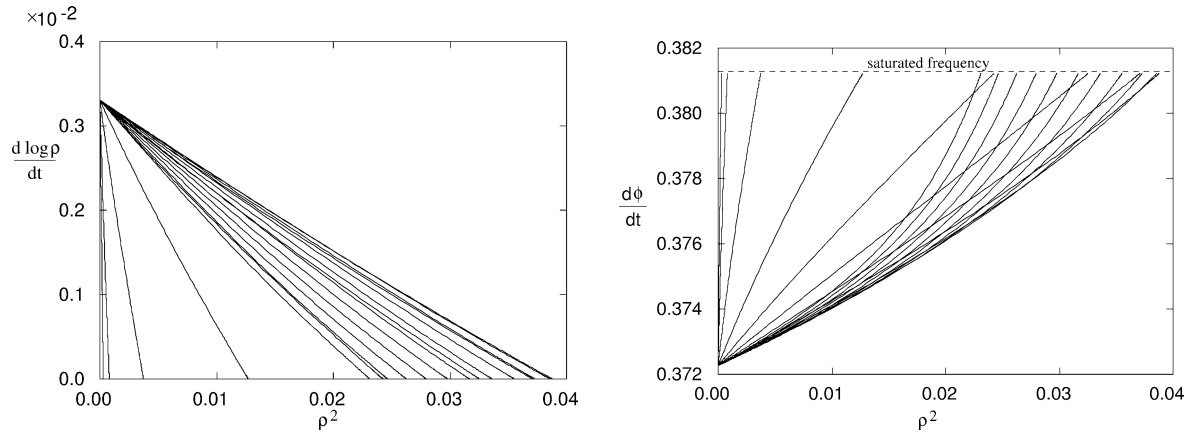


Fig. 2. Left: variation of $d \log(\rho)/dt$ with ρ^2 ; right: variation of $\dot{\phi}$ with ρ^2 . The different curves correspond to the different sampling positions on the wake centreline as described in the text. The initial and final values of both $d \log(\rho)/dt$ and $\dot{\phi}$ are both position independent.

3.2. Simulations at slightly post-critical Reynolds numbers

Simulations were performed at a number of Reynolds numbers exceeding the critical Reynolds number, however, for the purpose of the present discussion we will focus on the $Re = 48$ case, which is representative of the general behaviour. The transition takes place naturally, from initiation through computer round-off error, without the need to add a random noise component. At this Reynolds number the shedding period is $16.48R/U_\infty$, hence it takes approximately two-hundred periods to grow from low levels to saturation. Note that the timestep was $0.01 R/U_\infty$, corresponding to 1648 timesteps per shedding cycle. For the analysis described below, the transverse velocity was recorded at the following positions on the wake centerline: $\zeta = x/R = 1.3, 2, 4, 7, 10.5, 14, 17.5, 21, 24.5, 28, 31.5, 35, 38.5, 42, 45.5, 49, 52.5, 56$. Because of the distinct difference in timescale between the shedding period and the instability growth timescale, these signals can be accurately analysed to evaluate the Landau model coefficients. To do this, the times and amplitudes of all local peaks and troughs are extracted using quadratic interpolation. Note that these total amplitudes are very close to the amplitudes of the fundamental modes as it can be observed in Figs. 6 and 4 of Dusek et al. [1]. This provides direct measures of $\rho(t)$ and $\phi(t)$. Next the derivatives on the left-hand sides of Eqs (3) and (4), $d \log \rho/dt$ and $\dot{\phi}$, are evaluated by central differences. This provides two sets of derivatives as a function of ρ^2 and time. From these data, a fourth-order least-squares fit is performed. The functional variation is not strong as can be seen from Figs. 2 (a) and (b), and a fourth-order fit captures the variation accurately. Note that if the cubic Landau model was exact, only a first-order fit would be required.

For each figure all curves start at the same point on the vertical axis. This indicates that the parameters γ and ω are indeed constants independent of position as expected. The wake can be viewed globally as undergoing a linear transition from an unstable base flow. Initially, a single mode corresponding to a single frequency becomes amplified and since the instability initially grows linearly the growth rate will be identical everywhere.

For both figures the sets of curves end at a constant ordinate after the flow saturates (as required by saturation). Clearly $d \log \rho/dt \rightarrow 0$ and $d\phi/dt \rightarrow \omega_{\text{sat}}$ (the position independent angular frequency at saturation) as $\rho \rightarrow \rho_{\text{sat}}$. The gradients of these curves correspond to the local values of the real and imaginary cubic parameters of the Landau equation. Clearly, those parameters are strongly dependent on position (as pointed out by Dusek et al. [1]). Unlike for Fig. 2(a), the gradients of the curves in Fig. 2(b) are relatively strong functions of amplitude.

The data can be further analysed to evaluate the Landau constant. This can be determined by plotting $c(\rho^2) = (d \log \rho/dt - \gamma)/(d\phi/dt - \omega)$ against ρ^2 for each point on the wake centreline. Here γ and ω are derived from a least-squares fit at each point. Fig. 3 shows this variation. Clearly, this plot shows that the Landau constant indeed approaches a position-independent constant as the flow saturates as is indicated by the theoretical analysis (Eq. (5)). When the flow is growing exponentially in the linear regime, the Landau constant is a strong function of position, varying between approximately -3 [19] close to the back of the cylinder to approximately -1 far downstream. At saturation $c_{\text{sat}} = -2.708$. This is consistent with the value found by Dusek et al. [1]. However, these authors found the Landau constant was only close to a constant independent of position and amplitude. The difference between the result here and the previous finding results from the different ways the Landau constant was evaluated. Dusek et al. [1] evaluated the Landau constant by performing a linear least-squares fit to estimate c_R and c_I with a long time series of data including a considerable period of time after the flow had saturated. This leads to a biasing of the parameters to their saturated values. Hence their estimated Landau constants at different downstream positions were close to the saturated position-independent value found here. Numerically they found a variation of about 3%. In contrast,

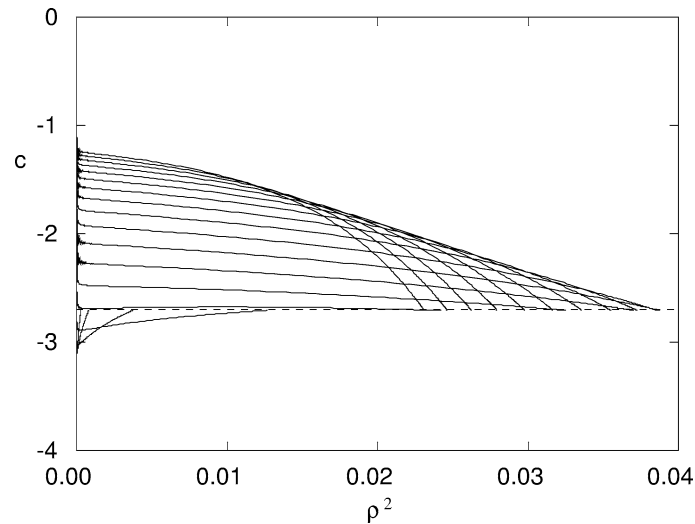


Fig. 3. Variation of the Landau constant with ρ^2 and position. The different curves correspond to different downstream positions on the wake centreline as given in the text. The curves end on the dashed line; the y-coordinate corresponds to c_{sat} . The curves are ordered with the position closest to the cylinder having the most negative initial c .

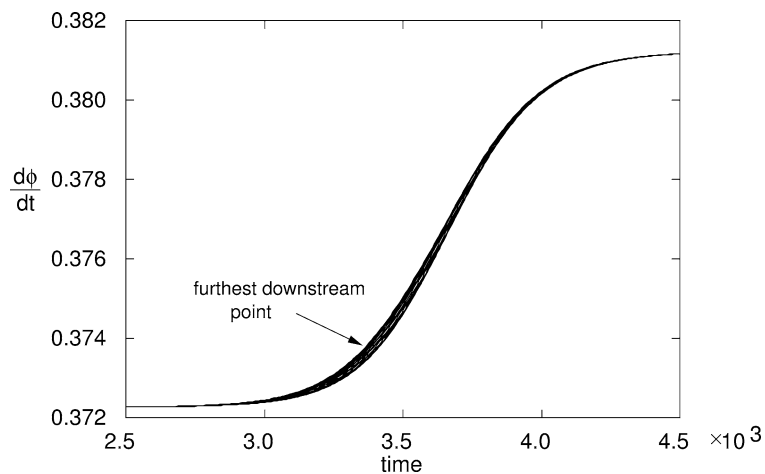


Fig. 4. Variation of the oscillation angular frequency with time at different points in the wake.

from the current numerical results, it is found that the Landau constant at saturation is position-independent to within 0.05% over the range ($1.3R < x < 56R$). This is within numerical error associated with the finite-differencing required. Of interest, at approximately $10R$ downstream the cylinder, the Landau constant remains approximately constant throughout linear growth and saturation. This explains in particular why experimentalists have been able to determine the Landau constant by direct velocity measurements during transients. Indeed, because of practical reasons, the highest velocity fluctuations were recorded with probes usually located between the cylinder and $10R$ downstream.

Fig. 4 shows the oscillation frequency ($d\phi/dt$) as a function of time at different points in the wake. This graph clearly shows the wake is locked during the linear growth phase, in line with theoretical analysis. In addition, since the oscillation frequency can be associated physically with the convection of the vortex street downstream, after saturation the wake must also be locked to a single frequency. This conclusion is also borne out by this figure, since post-saturation the velocities at all points are again oscillating at the same angular frequency. During the saturation phase, there is some minor variation of the oscillation frequency with position. This does not indicate that the wake loses coherence, but rather that readjustment is required to transform from one state (amplitude distribution) to another. This is probably due to several factors. The first is that the perturbation mode shape changes considerably during development from the linear phase to the saturated phase. The second is that the convection velocity variation with downstream distance also changes considerably between the linear and saturation

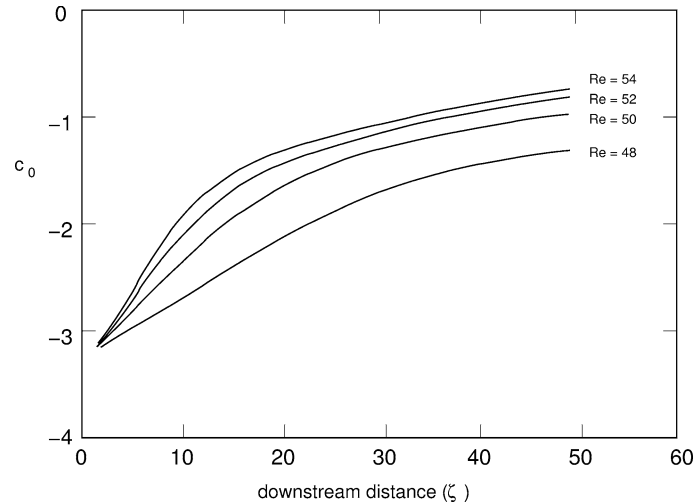


Fig. 5. Variation of initial Landau constant (c_0) with downstream position and Reynolds number.

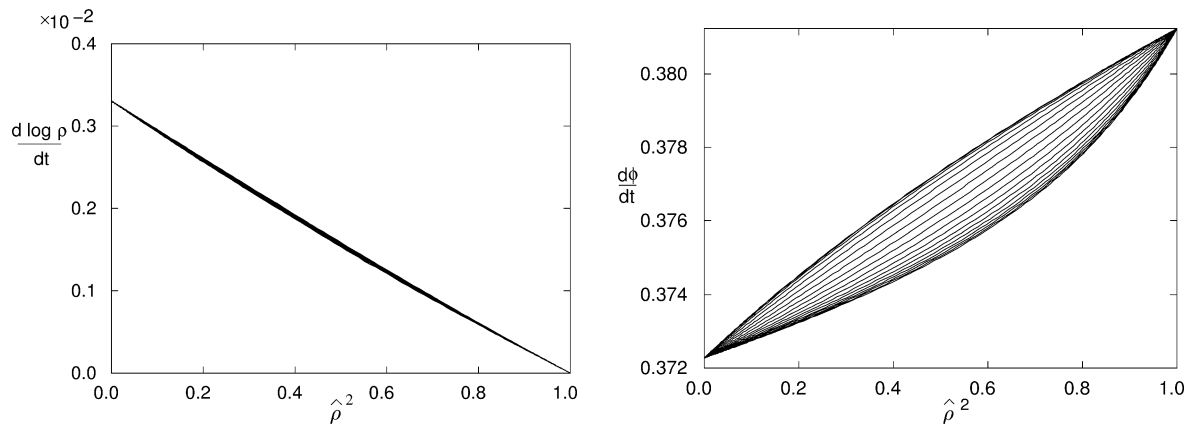


Fig. 6. Left: variation of $d \log(\rho)/dt$ with the scaled squared amplitude $\hat{\rho}^2$. Right: variation of $d\phi/dt$ with $\hat{\rho}^2$. The different curves correspond to the different sampling positions.

phases. Finally, any change in the oscillation frequency in the near wake is effectively convected downstream. This will result in a time lag between the near and far wake behaviour. However, Fig. 4 indicates that the frequency shift first occurs at points in the wake further downstream, hence the last factor certainly cannot dominate.

Fig. 5 shows the variation of the Landau constant during the initial linear growth phase (i.e., $c_0(\zeta) \equiv c(\rho^2 = 0, \zeta)$) as a function of downstream distance and also for a number of different post-critical Reynolds numbers. This data has been extracted by performing a fifth-order least-squares fit to the curves shown in Fig. 3 to extract the y-intercept. This shows explicitly the considerable spatial dependence of c_0 with position. Recall that c_0 corresponds to the (zero-amplitude) Landau constant of the semi-infinite Stuart–Landau model expansion, i.e., the model including higher-order terms not merely the third-order term.

Fig. 2(a) shows there is considerable variation of $d \log \rho / dt$ with position, however, in terms of the scaled squared amplitude ($\hat{\rho}^2 = \rho^2 / \rho_{\text{sat}}^2$), there is very little variation. This is shown in Fig. 6(a). Here, for each point, the amplitude is scaled by the value at saturation. All of the 18 curves are almost coincident. On the other hand, the same is not true for $d\phi/dt$, as is shown in Fig. 6(b). In this case there is considerable variation.

From Eq. (3), and using the result $\rho_{\text{sat}}^2 = \gamma / c_{R\text{sat}}$, we can derive an equation for the scaled amplitude ($\hat{\rho}$)

$$\frac{d \log \hat{\rho}}{dt} = \gamma (1 - \hat{c}_R(\hat{\rho}^2, \zeta)) \hat{\rho}^2. \quad (6)$$

Here, $\hat{c}_R \equiv c_R / c_{R\text{sat}}$; i.e., it is the scaled real cubic coefficient. The formal dependence on $\hat{\rho}^2$ and ζ have been made explicit in Eq. (6), however, Fig. 6(a) shows that the dependence on both variables is weak. Note that \hat{c}_R is just the local gradient of each

curve. Determination of the slope for each downstream position as a function of amplitude indicates that the variation during saturation is about 10% and the variation at different downstream positions is within 5% of the mean.

Now, Eq. (6) can be applied at any point (at least on the wake centreline), and the numerical results indicate that the function $\hat{c}_R(\hat{\rho}^2)$ varies by less than 10% between points close to the back of the cylinder and up to at least 30D downstream. Given the functional variation of \hat{c}_R , this equation could be solved explicitly to give $\hat{\rho}^2 = f(t)$, where f is almost position-independent. The differential equation also has the property that it is invariant to arbitrary shifts in time. This means that the different constants of integration at different points merely shift this near-universal function in time. This is demonstrated from the numerical results by plotting $\hat{\rho}^2$ against time for the different downstream locations as shown in Fig. 7. The analysis indicates that each curve should be close to self-similar, but merely shifted in time. This is demonstrated clearly in this figure.

Next, the implications of Eq. (5) can be further revealed by writing it in the form

$$\Delta\omega = \dot{\phi} - \omega = \gamma \frac{c_I}{c_R} \frac{c_R}{c_{R\text{sat}}} \hat{\rho}^2 = c(\hat{\rho}^2) \hat{c}_R(\hat{\rho}^2) \hat{\rho}^2. \tag{7}$$

Here, the dependence of the Landau constant c is explicitly written as a function of $\hat{\rho}^2$, as is explicitly shown in Fig. 3. Fig. 4 shows that there is only slight variation in the change in the frequency of oscillation at different points in the wake at least during the period when the cubic terms are becoming important. (From Fig. 4 this occurs for $t > 3500$.) Thus, at different points, we expect that $\Delta\omega$ will be approximately constant. Taking this assumption, and the empirical finding that \hat{c}_R is also approximately constant, Eq. (7) can be used to approximately relate the Landau constants at different points (say, ζ_1 and ζ_2)

$$c(\hat{\rho}^2, \zeta_1) / c(\hat{\rho}^2, \zeta_2) \simeq \hat{\rho}^2(\zeta_2) / \hat{\rho}^2(\zeta_1). \tag{8}$$

Thus within the framework of the cubic Landau model, the Landau constant must vary with amplitude because of the mode deformation which occurs during saturation and this effect is substantial.

Table 1 summarises the key parameters at different Reynolds numbers.

3.3. Stuart–Landau model results for the lift coefficient

During the simulations the lift coefficient per unit length was also recorded. This allows us to investigate how the Stuart–Landau model applies to an alternative amplitude variable. Prior to transition the lift is identically zero, hence this can be used

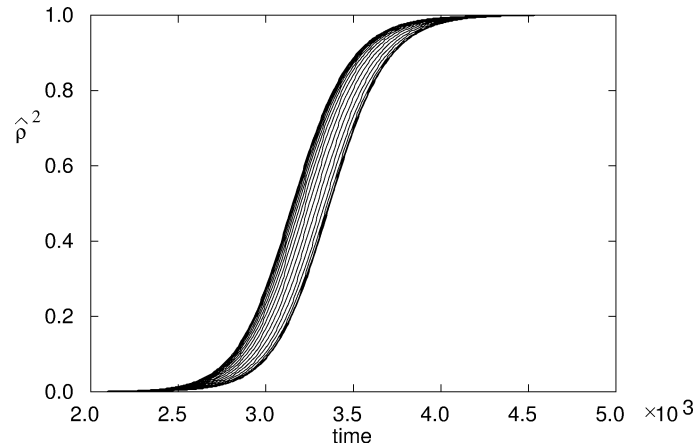


Fig. 7. Variation of $\hat{\rho}^2$ with time at different downstream positions. Each curve has approximately the same shape but is shifted in time.

Table 1
Key parameters of the Stuart–Landau model for the cylinder wake transition

Re	c_{sat}	γ	ω
46.7	−3.04	0.000613	0.37135
48	−2.71	0.003307	0.37227
50	−2.48	0.007271	0.37352
52	−2.36	0.011030	0.37457
54	−2.29	0.014594	0.37545

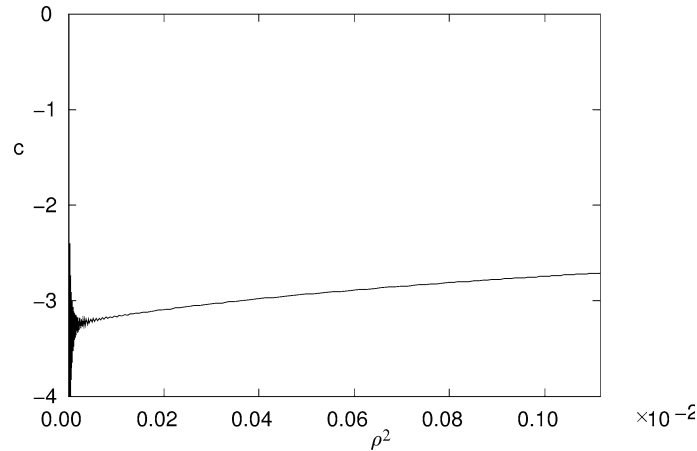


Fig. 8. Variation of the Landau constant with ρ^2 .

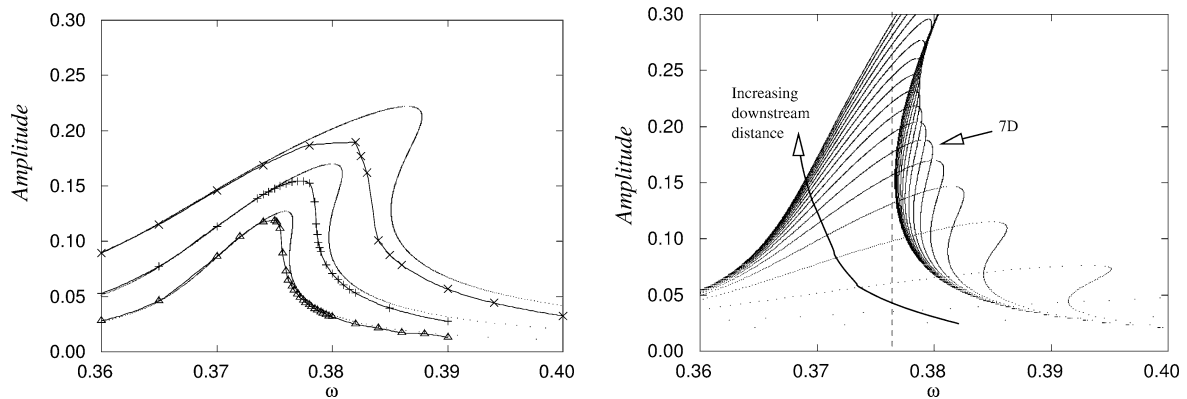


Fig. 9. Left: predicted resonance curves. The symbols denote resonance points determined by the numerical simulations. From lowest to highest the curves correspond to forcing levels of $U_{\text{pert}}/U_{\infty} = 0.025, 0.05$ and 0.1% . Also shown are the corresponding predicted resonance curves from the forced Landau model. The amplitude corresponds to the transverse velocity component at $7D$ downstream of the cylinder. Right: predicted resonance curves from the forced Stuart–Landau model as a function of downstream distance using measured local values of the parameters in the Landau equation.

as a direct (and perhaps global) measure of the growth of the instability. The identical analysis to that described above was applied to the force measurements. The analysis shows that γ , ω and c_{sat} are identical to within roundoff error. The variation of the Landau constant with ρ^2 is given in Fig. 8. The Landau constant for small amplitudes is similar to that recorded for the transverse velocity immediately at the base of the cylinder. Thus, perhaps not surprisingly, the response of the lift mirrors the response of the wake in the immediate vicinity of the back of the cylinder.

3.4. Forced Stuart–Landau model applied to a transversely oscillating cylinder at subcritical Reynolds numbers

Le Gal et al. [23], and Thompson and Le Gal [25] examined the response of the circular cylinder wake due to an applied transverse sinusoidal oscillation at the side boundaries at Reynolds numbers slightly below the critical value for shedding. In this case, the Stuart–Landau model can be extended to include a forcing term [23] modelling the effect on the wake of the transverse oscillation. It is possible to predict the detailed wake response using mathematical analysis. A key finding is that the wake should exhibit hysteresis above a critical oscillation amplitude provided the Landau constant is less than the critical value of $c_{\text{crit}} = -\sqrt{3}$. Thus, if the wake responds *globally* according to the forced Stuart–Landau model a hysteretic wake response should be observed if the forcing frequency is slowly increased and then decreased across the hysteretic range. Despite searching for this hysteresis effect both experimentally and numerically, it could not be found [23,9]. However, tantalisingly, the response curves showed the characteristic hysteretic loop shape except that the hysteretic frequency range was absent. This behaviour is shown in Fig. 9(a).

An interpretation of amplitude-frequency response is that the wake does not necessarily act as a global oscillator with a *constant* single Landau constant. The results in this paper indicate that Landau constant varies with position in the wake prior to saturation and it is only at saturation that the Landau constant is identical everywhere. This is really a constraint imposed by imposing the cubic Landau model. On the other hand, if a forcing term is added to the model so that the governing equation is

$$\frac{dA}{dt} = (\gamma + i\omega)A - (c_R + ic_I)|A|^2A + F \exp(i\Omega t), \quad (9)$$

then a similar analysis to that given above gives

$$0 = \gamma - c_R \rho_{\text{sat}}^2 + \frac{F}{\rho_{\text{sat}}} \cos(\delta), \quad (10)$$

$$\Omega = \omega - c_I \rho_{\text{sat}}^2 + \frac{F}{\rho_{\text{sat}}} \sin(\delta). \quad (11)$$

Here δ is the equilibrium phase lag, i.e., $(\Omega t - \phi)$, the difference between the forcing and response phases. This equation can be rearranged to give:

$$c = \frac{c_I}{c_R} = \frac{-\Omega + \omega + (F/\rho_{\text{sat}}) \sin(\delta)}{\gamma + (F/\rho_{\text{sat}}) \cos(\delta)}. \quad (12)$$

The phase δ varies with downstream distance. Consider two points in the wake with different downstream positions but with the same phase and hence the same δ . Since Ω , ω , γ and F are position-independent, but the saturated amplitude is *not* position-independent (within the framework of the Landau model) this equation indicates that these two points must have different Landau constants (even at saturation). Since the hysteretic frequency range of the response curve depends on the value of the Landau constant, if it varies with downstream distance, then the hysteretic ranges at different downstream positions do not match, and if there is no common overlap, then hysteresis should not be expected.

The predicted response curves at different downstream monitoring points obtained from the forced Stuart–Landau model are shown in Fig. 9(b). To obtain these curves, the unforced cylinder wake at a Reynolds number of 47 was evolved until it reached its equilibrium periodic state. At that stage the Reynolds number was reduced to $Re = 44$, below the critical value for the Hopf bifurcation at $Re_{\text{crit}} = 46.4$, and the flow was subsequently evolved while the wake oscillation decayed. It was found that after approximately one hundred periods, the initial transients decayed and the Landau constant at different downstream positions slowly relaxed to the zero-amplitude values. At each monitoring point, the variation of the Landau constant with local mode amplitude was fitted using a Padé approximant. Next these functional fits were used to predict the resonance curves shown in Fig. 9(b). These clearly show that the hysteretic frequency range depends on downstream position and furthermore that there is no common overlap region. Thus, the hysteresis range is effectively smoothed out as at some downstream points a high-amplitude flow state is predicted, while at others, a low-amplitude state is predicted. However, at higher and lower frequencies, the predicted wake state is single-valued and hence away from the virtual hysteresis range the response curves resemble the theoretical response curves as shown in Fig. 9(a).

4. Discussion and conclusions

Accurate numerical simulations have been used to analyse the applicability of the Stuart–Landau model to the initial Hopf bifurcation of the wake of the circular cylinder. While previous numerical and experimental results have indicated that the model appears to work remarkably well, a closer examination reveals that the story is more complex. For example, Dusek et al. [1] found that, if the Landau model variable is taken as the transverse velocity on the centreline, the Landau *constant* is position independent to within about 3% over a range of different positions in the wake. We find that the value they found corresponds to what we have called the Landau constant at saturation (c_{sat}). Here we focus on the truncated cubic Stuart–Landau model and allow higher-order terms to be accounted for by allowing the complex cubic coefficient to be a function of amplitude. In this case, simple analysis, with a few physically realistic assumptions (mainly phase-locking during the linear growth phases and after saturation), indicate that c_{sat} must be a constant independent of position (although still dependent on Reynolds number). The numerical results bear this out to within numerical error. On the other hand, the initial Landau constant (c_0), i.e., the value straight after the linear growth phase when cubic terms start to be important, is far from constant and is found to vary with position by a factor of approximately 3. Importantly, this parameter is really the mathematical Landau constant corresponding to the semi-infinite Stuart–Landau model containing odd terms in the amplitude that has been treated previously analytically.

The results have enabled us to analyse near universal (i.e., position-independent) behaviour of the wake. It is shown that the oscillation frequency shows only very minor variation with position at any time during the growth and saturation of the instability. In addition, while the real (c_R) and imaginary (c_I) coefficients of the cubic term in the model vary considerably

with position, if c_R is scaled by its value at saturation ($c_{R\text{sat}}$), then that function (\hat{c}_R) is almost position-independent and only weakly dependent on scaled squared amplitude ($\hat{\rho}^2$). The results also show that the variation of the scaled squared amplitude ($\hat{\rho}^2$) with time at different positions shows a universal behaviour, with curves corresponding to different positions only shifted in time. This can be explained by the theory given the empirical invariance of \hat{c}_R . Finally, we show that the variation of the initial Landau constant (c_0) with position, is (at least) partially associated with the mode deformation which occurs between the linear and post-saturation phases.

These results apply to a local wake variable (the transverse velocity) rather than a global variable (as perhaps the model was suggested for). To investigate the applicability of these results to a global variable, the Stuart–Landau model was examined also using the lift coefficient per unit length of the cylinder as the Landau model variable. In so far as the local results can be carried across, they apply to the analysis using the lift coefficient. For example, post-saturation c_{sat} is the same constant as for the local analysis. There is also non-negligible variation of the Landau constant with amplitude during the saturation phase as there was for the transverse velocity. The near constancy of the real coefficient \hat{c}_R is maintained, as is the universality of the variation of scaled amplitude with time. Interestingly, the variation of $c(\hat{\rho}^2)$ with $\hat{\rho}^2$ follows the variation for the transverse velocity component close to the base of the cylinder, (rather than the mean behaviour). Finally, an interpretation of the failure of the Landau equation when used to model the forced wake is given. We show that it is the variation of the Landau constant with the amplitude of the velocity oscillations in the wake that changes the shape of the resonance curves for each downstream position. Thus, whereas hysteretic loops are locally permitted, this effect is smoothed out by the spatial coherence of the wake.

References

- [1] J. Dusek, P. Le Gal, P. Fraunié, A numerical and theoretical study of the first Hopf bifurcation in a cylinder wake, *J. Fluid Mech.* 264 (1994) 59–80.
- [2] K.R. Sreenivasan, P.J. Strykowski, D.J. Olinger, Hopf bifurcation, Landau equation, and vortex shedding behind circular cylinders, in: K.N. Ghia (Ed.), *Proc. Forum on Unsteady Flow Separation*, vol. 52, ASME FED, 1986, pp. 1–13.
- [3] M. Provansal, C. Mathis, L. Boyer, Bénard–von Karman instability: transient and forced regimes, *J. Fluid Mech.* 182 (1987) 1–22.
- [4] M. Schumm, E. Berger, P. Monkewitz, Self-excited oscillations in the wake of two-dimensional bluff bodies and their control, *J. Fluid Mech.* 271 (1994) 17–53.
- [5] P. Albarède, M. Provansal, Quasi-periodic cylinder wakes and the Ginzburg–Landau model, *J. Fluid Mech.* 291 (1995) 191–222.
- [6] B.J.A. Zielinska, J.E. Wesfreid, On the spatial structure of global modes in wake flow, *Phys. Fluids* 7 (1995) 1418–1424.
- [7] R.H. Margarvey, R.L. Bishop, Transition ranges for three-dimensional wakes, *Canad. J. Phys.* 39 (1961) 1418–1422.
- [8] R.H. Margarvey, R.L. Bishop, Wakes in liquid–liquid systems, *Phys. Fluids* 4 (7) (1961) 800–805.
- [9] M.C. Thompson, T. Leweke, M. Provansal, Kinematics and dynamics of sphere wake transition, *J. Fluids Structures* 15 (2001) 575–585.
- [10] M. Provansal, D. Ormières, Étude expérimentale de l’instabilité du sillage d’une sphère, *C. R. Acad. Sci. Paris, Ser. IIB* 326 (1998) 489–494.
- [11] D. Ormières, M. Provansal, Transition to turbulence in the wake of a sphere, *Phys. Rev. Lett.* 83 (1999) 80–83.
- [12] B. Ghidersa, J. Dusek, Breaking of axisymmetry and onset of unsteadiness in the wake of a sphere, *J. Fluid Mech.* 423 (2000) 33–69.
- [13] D. Barkley, R.D. Henderson, Secondary instability in the wake of a circular cylinder, *Phys. Fluids* 8 (1996) 1683–1685.
- [14] R.D. Henderson, Nonlinear dynamics and pattern formation in turbulent wake transition, *J. Fluid Mech.* 352 (1997) 65–112.
- [15] C.H.K. Williamson, The existence of two stages in the transition to three-dimensionality of a cylinder wake, *Phys. Fluids* 31 (1988) 3165–3168.
- [16] R.D. Henderson, Details of the drag curve near the onset of vortex shedding, *Phys. Fluids* 7 (1995) 2102–2104.
- [17] I. Peshard, P. Le Gal, Coupled wakes of cylinders, *Phys. Rev. Lett.* 77 (1996) 3122–3125.
- [18] L. Schouveiler, A. Brydon, T. Leweke, M.C. Thompson, Interactions of the wakes of two spheres placed side by side, *Eur. J. Mech. B Fluids* 23 (2003).
- [19] P. Albarède, P. Monkewitz, A model for the formation of oblique shedding and “chevron” patterns in cylinder wakes, *Phys. Fluids A* 4 (1992) 744–756.
- [20] C.H.K. Williamson, Three-dimensional wake transition, *J. Fluid Mech.* 328 (1996) 345–407.
- [21] K. Roussopoulos, P. Monkewitz, Nonlinear modelling of vortex shedding control in cylinder wakes, *Physica D* 97 (1996) 264–273.
- [22] D. Barkley, L.S. Tuckerman, M. Golubitsky, Bifurcation theory for three-dimensional flow in the wake of a circular cylinder, *Phys. Rev. E* 61 (2000) 5247–5252.
- [23] P. Le Gal, A. Nadim, M.C. Thompson Hysteresis in the forced Stuart–Landau equation: application to vortex shedding from an oscillating cylinder, *J. Fluids Structures* 15 (2001) 445–457.
- [24] J.M. Gambaudou, Perturbation of a Hopf bifurcation by an external time-periodic forcing, *J. Differential Equations* 57 (1985) 172–199.
- [25] M.C. Thompson, P. Le Gal, Application of the forced Stuart–Landau model to cylinder wake oscillation, in: *Proceedings of the 14th Australian Fluid Mechanics Conference*, Adelaide, Australia, 10–14 December, 2001.
- [26] M.C. Thompson, K. Hourigan, J. Sheridan, Three-Dimensional Instabilities in the Wake of a Circular Cylinder, *Exp. Therm. Fluid Sci.* 12 (1996) 190.
- [27] G. Karniadakis, S. Sherwin, *Spectral-Element Methods for CFD*, Oxford University Press, New York, 1999.